



PCCP

**Growth and auto-oxidation of Pd on single-layer
AgO_x/Ag(111)**

Journal:	<i>Physical Chemistry Chemical Physics</i>
Manuscript ID	CP-ART-12-2019-006973.R1
Article Type:	Paper
Date Submitted by the Author:	15-Feb-2020
Complete List of Authors:	Mehar, Vikram; Univ Florida, Chemical Engineering O'Connor, Christopher; Harvard University, Chemistry and Chemical Biology Egle, Tobias; Harvard University, Chemistry and Chemical Biology Karatok, Mustafa; Harvard University, Chemistry and Chemical Biology Madix, Robert; Harvard University, School of Engineering and Applied Science Friend, Cynthia; Harvard University, Chemistry and Chemical Biology; Harvard University, Rowland Institute Weaver, Jason; Univ Florida, Chemical Engineering; University of Florida

SCHOLARONE™
Manuscripts

Growth and auto-oxidation of Pd on single-layer AgO_x/Ag(111)

Vikram Mehar¹, Christopher R. O'Connor², Tobias Egle^{2,3}, Mustafa Karatok², Robert J. Madix³,
Cynthia M. Friend^{2,3} and Jason F. Weaver^{1*}

¹Department of Chemical Engineering, University of Florida, Gainesville, FL 32611, USA

²Department of Chemistry and Chemical Biology, Harvard University, Cambridge, MA 02138, USA

³School of Engineering and Applied Sciences, Harvard University, Cambridge, MA 02138, USA

*To whom correspondence should be addressed, weaver@che.ufl.edu

Tel. 352-392-0869, Fax. 352-392-9513

Abstract

We investigated the growth and auto-oxidation of Pd deposited onto a AgO_x single-layer on $\text{Ag}(111)$ using scanning tunneling microscopy (STM) and X-ray photoelectron spectroscopy (XPS). Palladium initially grows as well-dispersed, single-layer clusters that adopt the same triangular shape and orientation of Ag_n units in the underlying AgO_x layer. Bi-layer clusters preferentially form upon increasing the Pd coverage to ~ 0.30 ML (monolayer) and continue to develop until aggregating and forming a nearly conformal Pd bi-layer at a coverage near 2 ML. Analysis of the STM images provides quantitative evidence of a transition from single to bi-layer Pd growth on the AgO_x layer, and a continuation of bi-layer growth with increasing Pd coverage from ~ 0.3 to 2 ML. XPS further demonstrates that the AgO_x layer efficiently transfers oxygen to Pd at 300 K, and that the fraction of Pd that oxidizes is approximately equal to the local oxygen coverage in the AgO_x layer for Pd coverages up to at least ~ 0.7 ML. Our results show that oxygen in the initial AgO_x layer mediates the growth and structural properties of Pd on the $\text{AgO}_x/\text{Ag}(111)$ surface, enabling the preparation of model PdAg surfaces with uniformly distributed single or bi-layer Pd clusters. Facile auto-oxidation of Pd by AgO_x further suggests that oxygen transfer from Ag to Pd could play a role in promoting oxidation chemistry of adsorbed molecules on PdAg surfaces.

Introduction

Applications of oxidation catalysis using alloys introduces the possibility that one or both of the metallic components transform to a metal-oxide(s) that acts as an active phase in promoting catalytic chemistry. An example is the complete oxidation of methane over PdPt alloys for which PdO serves as the active phase for methane oxidation.^{1, 2} Alloys of Pd with Ag or other coinage metals are also promising as catalysts for oxidation chemistry. Palladium forms an oxide that is highly active in promoting the dehydrogenation and complete oxidation of hydrocarbons and other compounds,³ while oxygen-covered Ag is active in promoting both partial and complete oxidative transformations of organic compounds, depending on the nature and concentration of oxygen on the Ag surface.⁴⁻⁸ The combination of Pd and Ag in a single material could effect selective oxidative transformations by a mechanism wherein PdO activates reactant molecules and the resulting intermediates migrate onto Ag sites and partially oxidize to generate value-added products.

Advancing the basic understanding of the behavior of PdAg surfaces under oxidizing conditions is important for guiding catalyst design. Prior studies show that PdAg surfaces can be highly dynamic at modest temperatures. For example, Pd atoms aggregate to form large islands on Ag(111) at room temperature, and heating to only 400 K in UHV is sufficient to promote the formation of a Ag capping layer on top of the Pd islands thereby lowering the surface free energy.⁹ Exposure to elevated pressures (~ 1 Torr) of O₂ draws Pd back to the surface of PdAg islands and produces Pd oxide structures even at 400 K due to the thermodynamic preference for Pd over Ag oxidation.⁹ Similarly, oxidation of a Pd₇₅Ag₂₅(100) alloy generates a PdO(101) single-layer that is separated by the stoichiometric bulk alloy by an Ag-rich interfacial layer.¹⁰ The formation of such an Ag-rich interface could influence the chemical properties of the PdO(101) surface, and

illustrates the potential for generating unique structures by oxidizing alloy surfaces. These prior studies show that the atomic distribution of PdAg surfaces can change dynamically in response to the reactive environment even at mild temperatures, and motivate investigations to further clarify how oxidizing conditions influence the structural and chemical properties of PdAg surfaces.

In the present study, we investigated the growth of Pd deposited onto a well-ordered AgO_x single-layer on Ag(111). A key aim of the work is to characterize the evolution of surface structure and oxidation states in a PdAg system that features an initial gradient in the oxygen chemical potential because the deposited metal (Pd) forms a more stable oxide than the metal-oxide support (AgO_x). We find that oxidizing Ag(111) enhances the adhesion of Pd to the surface and strongly influences the morphology and chemical nature of the deposited Pd. Our results show that oxygen migration from Ag to Pd is facile and may play a role in mediating chemical processes on PdAg surfaces.

Experimental Details

Scanning tunneling microscopy (STM) measurements were performed in an ultrahigh vacuum (UHV) system described previously.¹¹ The UHV chamber is equipped with a scanning tunneling microscope (RHK), a four-grid retarding field analyzer (SPECS) for low-energy electron diffraction (LEED) and Auger electron spectroscopy (AES), a quadrupole mass spectrometer (QMS) (Hiden), a Fourier transform infrared spectrometer (FTIR) system, an ion sputter gun, and an electron-beam metal evaporator (McAllister Technical Services) for vapor deposition of Pd. The equipment used for scanning tunneling microscopy (STM) was produced by RHK and includes a UHV 300 “beetle-type” scan head operated with an SPM 100 controller. A single-stage

differentially pumped chamber¹² is also attached to the main UHV chamber which houses an inductively coupled RF plasma source that is used to generate atomic oxygen beams.

The Ag(111) crystal used in this study is a circular top-hat-shaped disk (10 mm × 1.65 mm) cut to isolate the (111) surface plane within a tolerance of $\pm 0.1^\circ$. The sample holder consists of a TiN-coated top ramp for STM tip approach with the sample sandwiched between sapphire washers and secured by tungsten leaf springs. The sample holder is cooled via thermally conductive contact between a copper braid and a liquid nitrogen reservoir. This design allows for radiative and e-beam heating of the sample to 800 K, cooling to 90 K, and full electrical isolation from electrical heating contacts to maintain a stable voltage bias for STM. The sample temperature was monitored with a type-K thermocouple attached to the bottom of the sample. Sample cleaning consisted of cycles of sputtering with 2000 eV Ar⁺ ions at a surface temperature of 300 K, followed by annealing at 800 K for 5 min in UHV. We considered the Ag(111) sample to be clean when Auger electron spectra exhibited no discernable signals for the C(KLL), S(KLL) and O(KLL) peaks and we observed a sharp LEED pattern characteristic of Ag(111).

A single-layer AgO_x film was grown by exposing the Ag(111) surface to an O-atom beam at a surface temperature of 500 K followed by heating to 520 K in UHV, as discussed below. Pd films of varying thickness were grown on the AgO_x/Ag(111) surface at 300 K by vapor depositing Pd (Alfa Aesar, 99.9%) using an electron-beam evaporator. The Pd coverage was calibrated by collecting AES spectra as a function of the Pd exposure to clean Ag(111) at 300 K, and relating the attenuation of the Ag MNN peak at 351 eV to the thickness of the Pd layer, assuming an inelastic mean free path (IMFP) of the Auger electrons through Pd of 7.05 Å as estimated by the Gries equation.¹³ Coverages of Pd are computed in units of ML by dividing the thickness estimated from the AES measurements with the monatomic step height on Pd(111) of 2.2 Å. An average Pd

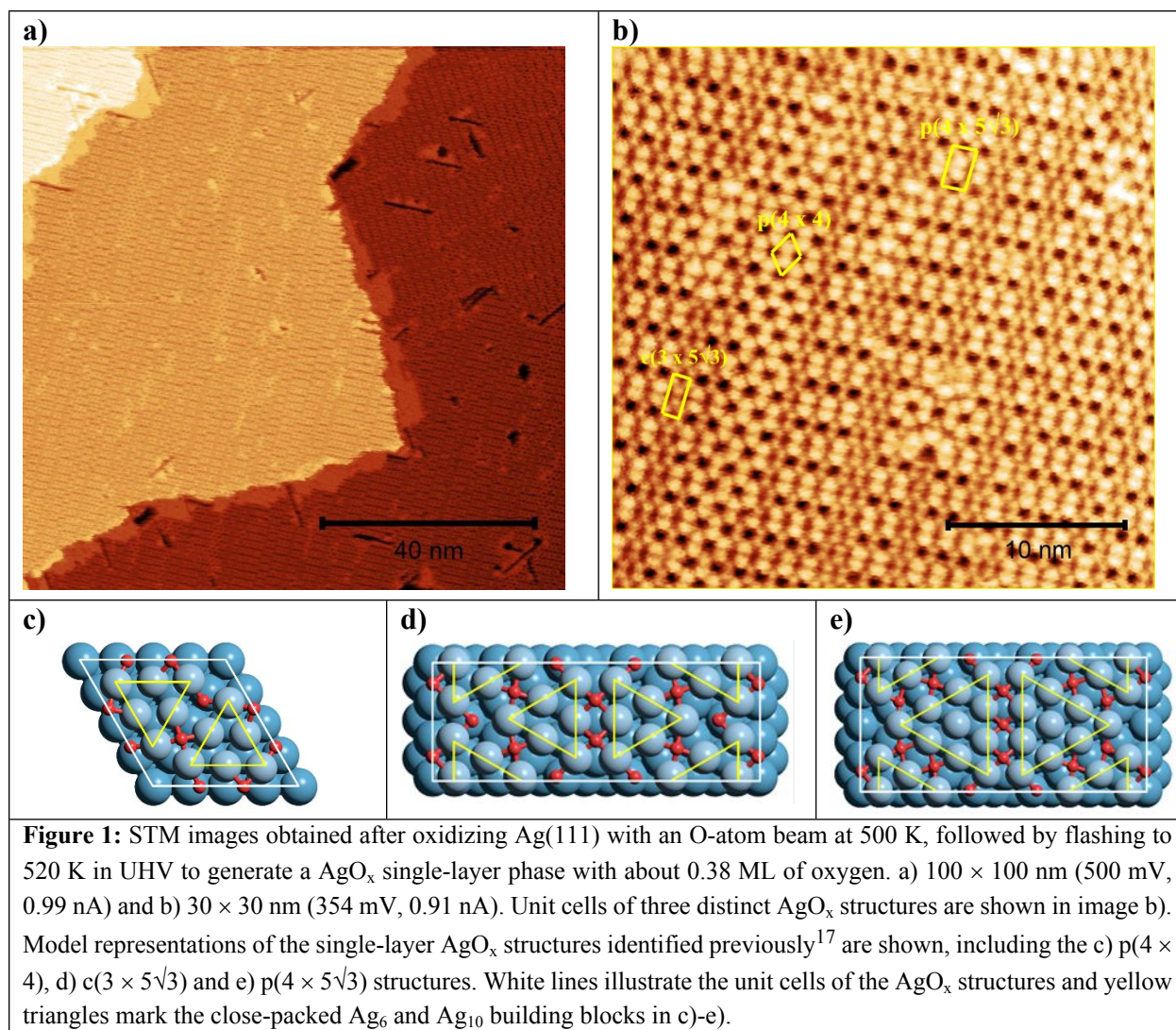
deposition rate of 0.075 ML/min is estimated for our measurements. STM measurements were performed at a sample temperature of ~ 300 K and the tunneling interaction was set to the constant current feedback mode. Images were collected at typical scan settings in the range of +0.2 to +0.5 V sample bias and a tunneling current of 0.5–1.2 nA.

XPS experiments were performed in an UHV chamber that has been described previously.⁹ The preparation chamber (base pressure $\sim 5 \times 10^{-10}$ Torr) contains an electron-beam evaporator (Focus EFM3) and a sputter gun (Perkin Elmer 04-161). The Ag(111) crystal was extensively cleaned by Ar⁺ sputtering (2 keV) followed by annealing to 790–800 K in UHV. Ozone (LG-7 Laboratory Ozone Generator) was directly dosed onto the Ag(111) crystal at 500 K, followed by a flash anneal to 520 K. LEED and O₂ TPD results (Figure S1, Supporting Information) provide evidence that the same AgO_x single-layer structure is generated by oxidizing with atomic oxygen or ozone at the temperatures employed. Pd was deposited at 300 K onto single-layer AgO_x/Ag(111) from a rod using the electron-beam evaporator. The Pd coverage was calibrated based on prior Pd/Ag ratios measured by XPS on a non-oxidized sample and assuming that all Pd remained on the surface at the deposition temperature of 300 K. For XPS measurements in the analysis chamber (base pressure $\sim 2 \times 10^{-10}$ Torr) an X-ray source using (non-monochromatized) Mg K α radiation was employed. The sample was irradiated under an angle of 45°, and the photoelectrons were measured at normal emission using a hemispherical analyzer, at a pass energy of 10 eV and in the large-area lens mode. The spectra acquired on Ag(111) and Pd/Ag(111) were fitted using a Doniach-Šunjić function¹⁴ convoluted with a Gaussian function and background lines obtained from Shirley's method.¹⁵

Results and Discussion

Single-layer AgO_x on Ag(111)

A single-layer AgO_x structure was prepared by oxidizing Ag(111) with an O-atom beam at 500 K, followed by flashing the surface to 520 K in UHV. This procedure generates large, atomically-flat domains of an AgO_x single layer (Figure 1a) that is comprised of a mixture of crystalline structures with O-coverages between 0.375 and 0.4 ML, consistent with prior studies.¹⁶⁻¹⁸ STM reveals that the AgO_x single layer is comprised of large domains of the rectangular $p(4 \times 5\sqrt{3})$ structure separated by 1-2 rows of the rectangular $c(3 \times 5\sqrt{3})$ structure as well as larger regions containing the hexagonal $p(4 \times 4)$ structure (Figure 1b). While the $p(4 \times 5\sqrt{3})$ structure is more prevalent, the $p(4 \times 4)$ structure and the $c(3 \times 5\sqrt{3})$ structure, to a lesser extent, are also present in significant quantities. It is worth noting that the LEED pattern obtained from the AgO_x layer generated at 500 K agrees well with the pattern simulated for the $c(3 \times 5\sqrt{3})$ structure, whereas the LEED pattern obtained after flashing to 520 K no longer exhibits distinguishing spots of the $c(3 \times 5\sqrt{3})$ structure and is instead characteristic of the $p(4 \times 5\sqrt{3})$ as well as the $p(4 \times 4)$ structure (see Figure S2). This finding is consistent with the domain sizes that we observe with STM as well as a recent study by Derouin et al.¹⁶ showing that the $p(4 \times 5\sqrt{3})$ structure is dominant after oxidizing Ag(111) with atomic oxygen at 525 K.



Prior work provides detailed information about the single-layer AgO_x structures that form on Ag(111), and show that generating pure phases of a given AgO_x structure is generally challenging.¹⁶⁻²¹ Schnadt et al.¹⁷ report that each of the single-layer AgO_x structures has a stoichiometry close to Ag_2O , and that the Ag and O coverages are specifically as follows; $p(4 \times 4)$: 0.75 ML and 0.375 ML, $p(4 \times 5\sqrt{3})$: 0.80 ML and 0.375 ML and $c(3 \times 5\sqrt{3})$: 0.80 ML and 0.40 ML. DFT calculations predict that the single-layer AgO_x phases have similar thermal stability,¹⁷ consistent with results of O_2 TPD experiments.^{16, 22} While the structures exhibit distinct long-range periodicity, each is comprised of a common structural motif consisting of triangular-shaped Ag_6

units that are formed from hexagonally close-packed Ag atoms and separated from one another by rows of O-atoms (Figure 1c-e).¹⁶⁻¹⁹ The $p(4 \times 5\sqrt{3})$ structure contains triangular Ag_{10} in addition to Ag_6 units.¹⁷ The edges of the Ag_n units align along close-packed $\langle 110 \rangle$ directions and the Ag atoms bond on top of either fcc or hcp hollow sites of the Ag(111) surface. Knowledge of these structural characteristics is important for understanding the initial growth of Pd on the AgO_x single-layer.

Surface morphology of Pd deposited onto $\text{AgO}_x/\text{Ag}(111)$

Figures 2a-d show wide-scale STM images (100×100 nm) obtained after depositing Pd onto single-layer $\text{AgO}_x/\text{Ag}(111)$ at 300 K to generate Pd coverages between 0.15 and 1.8 ML. The images show that Pd deposition initially produces small domains (1 to 3 nm) that disperse uniformly across the surface. These characteristics contrast sharply with reports that Pd agglomerates into large islands on clean Ag(111) and tends to accumulate at step edges.⁹ An implication is that Pd interacts favorably with the AgO_x phase, and that the strong Pd- AgO_x interaction suppresses Pd surface mobility and agglomeration and instead promotes the nucleation of Pd domains uniformly across the surface. The Pd continues to wet the AgO_x layer as the Pd coverage increases, and forms larger domains that transform into a nearly conformal layer at a Pd coverage of 1.8 ML. High resolution images further show that the characteristic heights and shapes of the Pd domains change abruptly as the Pd coverage increases above ~ 0.15 ML, and suggest a change from single to bi-layer Pd growth.

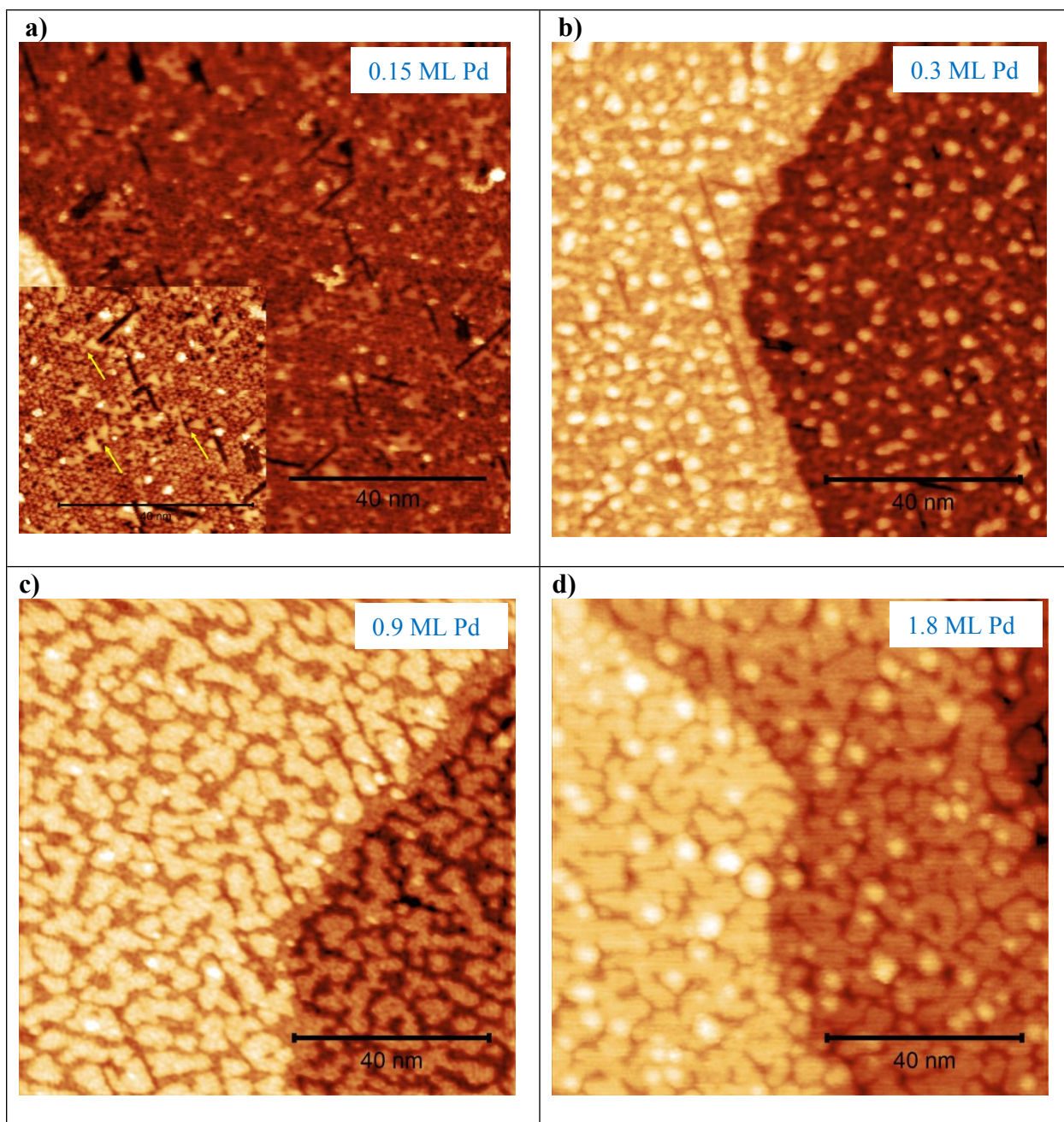
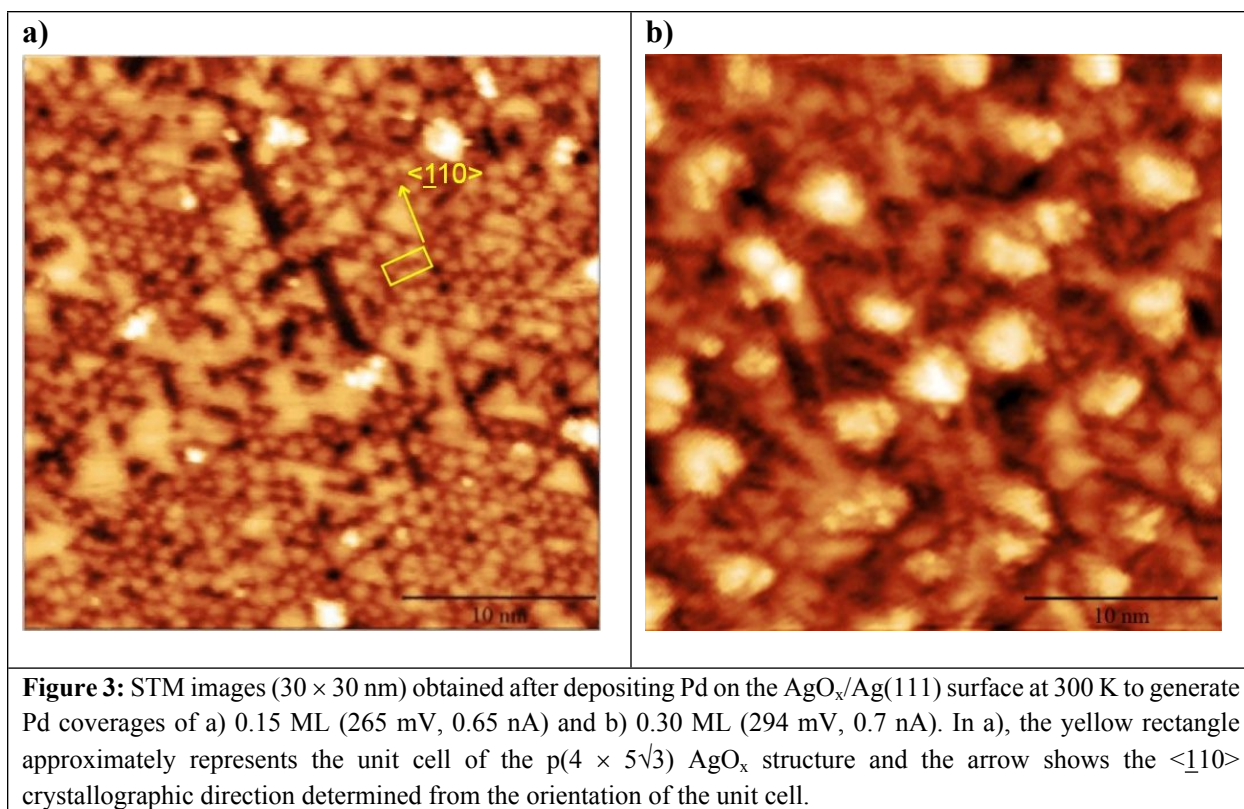


Figure 2: STM images (100×100 nm) obtained after depositing Pd on the AgOx/Ag(111) surface at 300 K to generate Pd coverages of a) 0.15 ML (265 mV, 0.65 nA), b) 0.30 ML (374 mV, 0.77 nA), c) 0.90 ML (366 mV, 1.2 nA) and d) 1.8 ML (241 mV, 0.98 nA). The inset of a) shows a (50×50 nm) image of the 0.15 ML Pd-AgOx/Ag(111) surface. The inset of a) shows a (50×50 nm) image that highlights selected triangular Pd structures (yellow arrows) that form after depositing 0.15 ML of Pd on AgOx/Ag(111).

High resolution images of Pd-AgO_x/Ag(111)

STM images show that low coverages of Pd (≤ 0.15 ML) predominantly grow as single-layer, triangular structures that align with the triangular Ag_n patches of the AgO_x layer. Figure 3a shows an atomically-resolved STM image (30 × 30 nm) obtained from a Pd-AgO_x/Ag(111) surface with 0.15 ML of Pd. The triangular Pd structures are oriented in specific directions and have an average apparent height and diameter of 0.08 nm and 1.4 nm, respectively. Triangular Pd structures of the same apparent height are also dominant at Pd coverages below 0.15 ML (Figure S3). The orientations of the Pd domains can be determined by reference to the surrounding AgO_x structure. The yellow rectangle drawn in Figure 3a approximately represents the unit cell of the $p(4 \times 5\sqrt{3})$ AgO_x structure, and is positioned near atomic features that exhibit local periodicity consistent with this structure. The short side of this unit cell (i.e., the $\langle 110 \rangle$ direction) is parallel to an edge of the triangular Pd structures observed in Figure 3a and is also parallel to an edge of the triangular Ag_n units that comprise the various AgO_x structures (Figures 1c-e). From this comparison, we conclude that the triangular Ag_n units serve as nucleation sites for Pd and impart their shape on the initial Pd structures that form.



The surface morphology as well as the sizes and shapes of the Pd clusters change significantly upon increasing the Pd coverage to 0.30 ML. Comparison of Figures 3a and b reveals that the Pd clusters generated at 0.30 ML exhibit brighter contrast than the triangular structures observed at lower Pd coverage. In fact, the average apparent height of these clusters is nearly twice that of the triangular structures (0.14 vs. 0.08 nm), consistent with a change from single to bi-layer growth. Although the measured apparent height difference is less than that of a monatomic step on Pd(111) (~ 0.6 vs. 2.0 Å), the underlying AgO_x layer may suppress the electronic corrugation that is measured perpendicular to the surface and cause the measured heights to be lower than the actual geometric heights. As discussed below, quantitative analysis of the morphological properties of the deposited Pd further supports the conclusion that the growth changes from single to bi-layer with increasing Pd coverage above ~ 0.15 ML.

The Pd clusters produced at 0.3 ML are also larger in diameter and form more irregular shapes compared with the triangular structures (Figure 3b vs. 3a), and the Pd cluster density is lower at 0.30 vs. 0.15 ML. The average diameter of the irregularly-shaped clusters is 2.7 nm, which is nearly twice that of the triangular structures, and the cluster density is more than four times higher at 0.15 vs. 0.3 ML. These differences indicate that Pd clusters on the AgO_x layer begin to ripen as the Pd coverage increases above ~ 0.15 ML and show that this ripening coincides with a transition from single to bi-layer Pd growth. The images also show that the surrounding AgO_x layer is more disordered after the deposition of 0.3 vs. 0.15 ML of Pd. This restructuring is consistent with partial reduction of the AgO_x layer induced by the Pd, as discussed below.

It is important to note that our STM images are insufficient for determining if the Pd domains are pure Pd or contain both Pd and Ag atoms since they lack atomic resolution of these domains. Prior studies report that Pd and Ag intermixing initiates above ~ 450 -500 K for Ag layers on Pd(111)²³⁻²⁶ as well as Pd deposits on Ag(111),⁹ and that the deposited metals remain nearly pure at lower temperature. These studies suggest that intermixing between Pd and Ag should occur negligibly at the temperature (300 K) at which we deposited Pd onto the AgO_x single-layer. However, our results reveal a strong interaction between Pd and the AgO_x phase that causes a significant amount of Pd to become partially oxidized by the AgO_x phase at 300 K. The Pd-induced reduction of the AgO_x layer could conceivably stimulate some intermixing of Pd and Ag at 300 K. Future investigations of the surface chemical properties may aid in determining if Ag atoms incorporate into the Pd domains of these Pd- AgO_x /Ag(111) surfaces.

STM image analysis

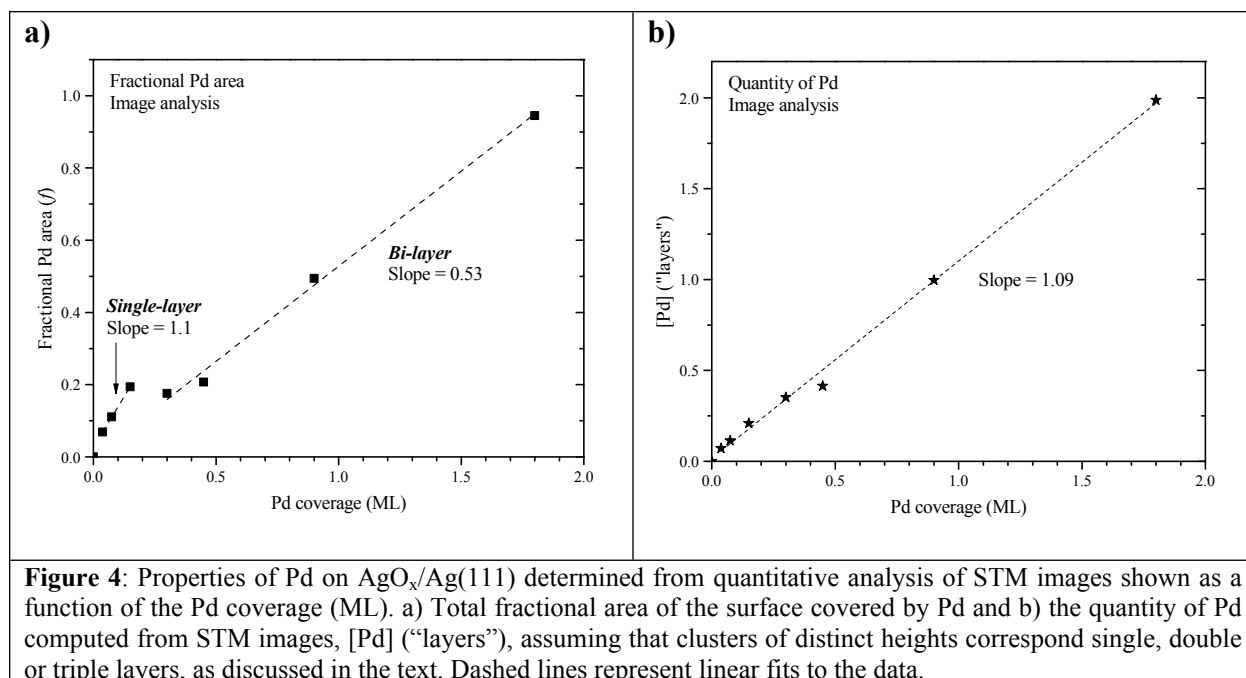
Table 1 summarizes morphological properties of Pd domains determined from analyzing STM images obtained at Pd coverages between 0.04 and 1.8 ML. The analysis identifies Pd clusters with three distinct heights (0.08, 0.14 and 0.25 nm), strongly suggestive of single, double and triple layers of Pd. Table 1 reports the total fractional area (f) covered by Pd domains at each Pd coverage, where f is defined as the sum of the fractional areas covered by each type of domain at a given Pd coverage. Additional details and results of the analysis are given in SI. It is important to note that single-layer Pd domains are not evident in images obtained at Pd coverages ≥ 0.30 ML but are also challenging to identify due to disordering in the AgO_x layer (Figure 3b). Single-layer Pd clusters are neglected in the analysis of images obtained at [Pd] ≥ 0.30 ML. The consequences of this omission are discussed below.

Table 1: Structural properties of Pd domains as a function of the total Pd coverage (ML) determined from statistical analysis of STM images. Structural properties listed in the table include the average height and diameter of Pd domains and the total fractional area of the surface covered by Pd domains (f). The average cluster diameter is computed by multiplying the average diameter of each type of cluster with the population of the cluster observed at a given Pd coverage. Average heights shown in Table 1 are also computed as a weighted average. The far right column lists the quantity of Pd (“layers”) computed as a weighted average, assuming that clusters with apparent heights of 0.08, 0.14 and 0.25 nm correspond to single, double and triple layers. Additional details are provided in the text and SI.				
Pd coverage (ML)	Average height (nm)	Average diameter (nm)	Fractional Pd area (f)	Quantity of Pd (“layers”) ($f_1 + 2f_2 + 3f_3$)
0.04	0.08	1.0	0.07	0.07
0.08	0.08	1.4	0.11	0.11
0.15	0.08	1.4	0.19	0.21
0.30	0.14	2.7	0.18	0.35
0.45	0.14	2.8	0.21	0.41
0.90	0.14	6.4	0.49	1.00
1.8	0.15	32.8	0.95	1.99

The analysis shows that the average cluster height is 0.08 nm for [Pd] ≤ 0.15 ML and remains nearly constant at 0.14 nm for Pd coverages from 0.30 to 1.8 ML. The average cluster heights computed for [Pd] ≥ 0.30 ML might be overestimated since the analysis omits possible

contributions from single-layer clusters at these coverages. The height analysis does show that the formation of Pd bi-layers is strongly preferred over the formation of thicker Pd clusters at coverages between 0.30 and 1.8 ML. The analysis also reveals that the average diameter of single-layer Pd clusters increases from 1.0 to 1.4 nm with increasing Pd coverage to 0.15 ML, while the average diameter of bi-layer clusters is initially near 2.7 nm and increases as the Pd domains aggregate into a more contiguous film as the Pd coverage approaches 1.8 ML.

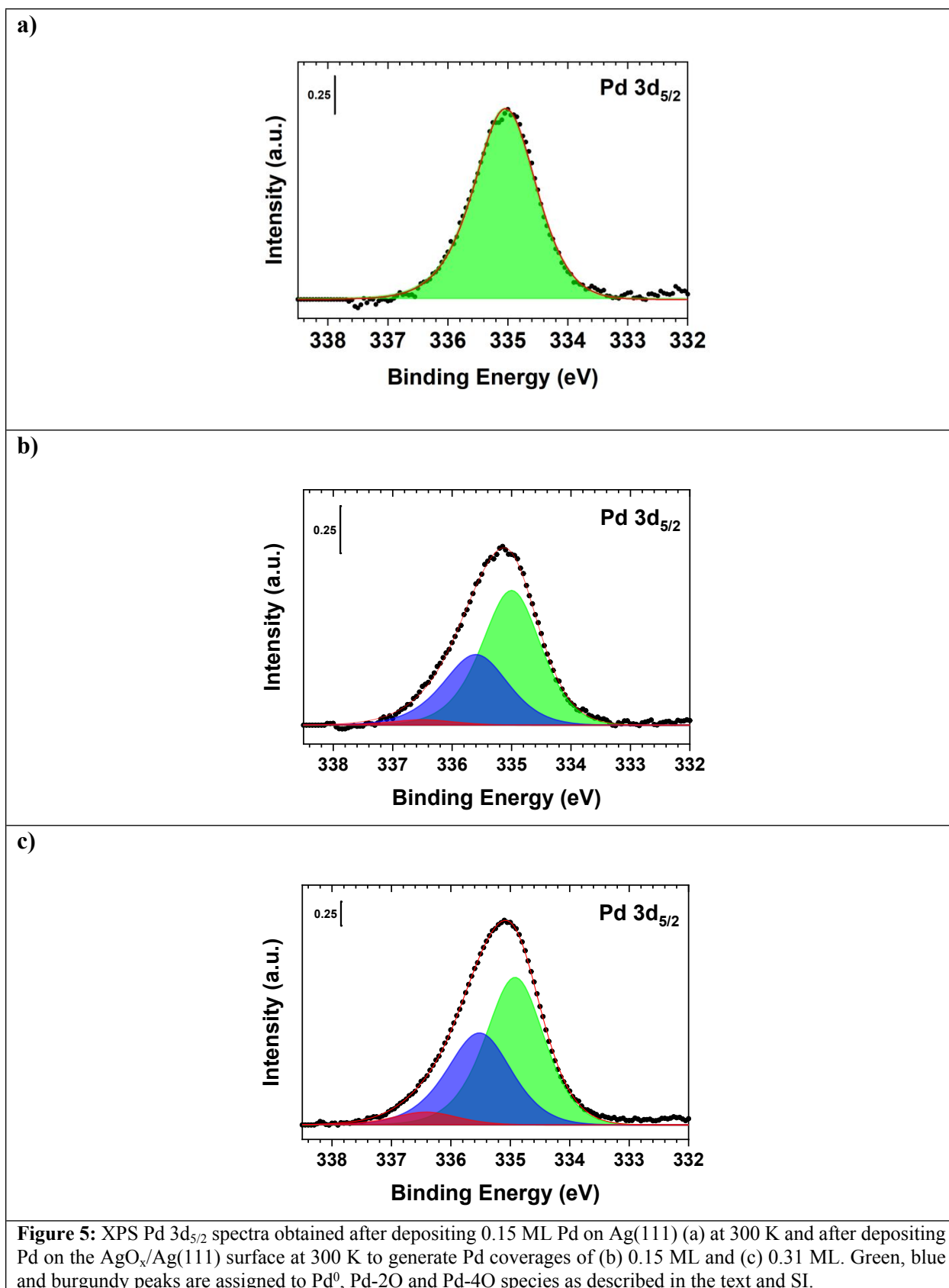
Figure 4a shows that the relationship between the fractional Pd area (f) and the Pd coverage is quantitatively consistent with a transition from single to bi-layer growth at a Pd coverage between 0.15 and 0.30 ML, followed by bi-layer growth thereafter. The f vs. [Pd] data exhibits two distinct linear regions. Below a Pd coverage of 0.15 ML, the f vs. [Pd] data can be accurately fit with a linear function with a slope of 1.1 (Figure 4a). This proportionality is consistent with the formation of single-layer Pd domains since Pd addition exclusively to the surface layer would cover a fractional area that is roughly equal to the quantity of close-packed Pd layers deposited, i.e., number of Pd ML. The fractional Pd area also increases linearly with increasing Pd coverage from 0.30 to 1.8 ML but with a slope equal to 0.53. This relation suggests that roughly half of the deposited Pd is exposed at the surface, and is thus consistent with Pd bi-layer growth at coverages above 0.30 ML.



The quantity of Pd was computed from the STM images to further test the assumption that clusters of distinct heights correspond to single, double and triple layers of Pd. For this calculation, the amount of Pd is determined from an average expressed as $[\text{Pd}]$ ("layers") = $f_1 + 2f_2 + 3f_3$ where f_1, f_2 and f_3 are the fractional areas of clusters with average heights of 0.08, 0.14 and 0.25 nm and the weighting factors 1, 2 and 3 represent the assumed number of Pd layers for each cluster height. The SI lists the values of f_1, f_2 and f_3 for each Pd coverage shown in Table S1. Table 1 and Figure 4b shows that the amount of Pd computed from the STM images agrees well with the Pd coverages estimated from AES, with [Pd] ("layers") following a single linear relation with a slope of 1.09 for the entire range of Pd coverages studied. Overall, the quantitative image analysis further supports the conclusion that Pd growth on the AgO_x single-layer undergoes a single to bi-layer transition as the Pd coverage increases above ~ 0.15 ML, and demonstrates that bi-layer formation continues preferentially until a nearly contiguous Pd film forms at 1.8 ML.

XPS characterization of Pd on AgO_x/Ag(111)

Characterization using XPS demonstrates that a fraction of the Pd atoms become partially oxidized immediately upon Pd deposition onto the AgO_x/Ag(111) surface at 300 K. Figures 5a,b,c show XPS Pd 3d_{5/2} spectra obtained after depositing 0.15 ML of Pd on Ag(111) as a reference and after depositing 0.15 and 0.31 ML of Pd onto single-layer AgO_x. Pd 3d_{5/2} spectra collected at other Pd coverages between 0.15 and 2.5 ML are shown in SI along with the C 1s, Ag 3d_{5/2} and O 1s spectral regions (SI, Figures S4 and S5). The O 1s spectra are challenging to interpret since they may exhibit components from multiple oxygen species and overlap with the Pd 3p_{3/2} peak. In contrast, the Pd 3d_{5/2} spectra can be fit with two main peaks representing Pd⁰ and Pd-2O as well as a smaller peak from more oxidized Pd-4O species for Pd coverages up to about 0.66 ML (see SI). The Pd-2O peak is consistent with Pd that bonds with chemisorbed O-atoms²⁷ and is significantly larger than the Pd-4O peak at all Pd coverages. Because CO adsorbed from the background becomes observable in the C 1s spectra at Pd coverages above ~1 ML, an additional peak is included in the fit of the Pd 3d_{5/2} spectra to represent Pd bonded to CO at higher Pd coverages (>~ 1 ML). The CO is present in relatively low coverages according to quantitative analysis of the Pd 3d_{5/2} spectra (Table S2) and is not expected to influence Pd growth.



Analysis of the Pd 3d spectra reveals that a large fraction of the Pd becomes partially oxidized by the single-layer AgO_x phase, confirming that Pd interacts strongly with the Ag oxide. Resolving the concomitant AgO_x reduction is challenging because Ag coordinated with Pd produces a Ag 3d peak with a similar binding energy as Ag oxides,⁹ shifted by only about 0.4 eV below that for metallic Ag,²⁸⁻³⁰ and the peak from metallic Ag dominates the spectra for the photon energy employed ($h\nu = 1253.6$ eV). The analysis shows that $61 \pm 3\%$ of the Pd is metallic for the range of Pd coverages studied (0.15 to 2.5 ML), while the remaining Pd is oxidized. The analysis further indicates that $38 \pm 4\%$ of the Pd coordinates with O-atoms after depositing up to 0.66 ML of Pd on the AgO_x/Ag(111) surface, and about 23% and 15% of the Pd bonds with O and CO, respectively, at Pd coverages of 1 and 2.5 ML. The fraction of oxidized Pd decreases below 38% in part because oxygen becomes the limiting reactant at Pd coverages above 1 ML. Overlap between the Pd 3d_{5/2} peaks also introduces greater uncertainty in estimating the relative quantities of the Pd-2O and Pd-CO species. Overall, the analysis demonstrates that a large quantity of Pd becomes partially oxidized by the AgO_x single-layer.

XPS shows that the fraction of Pd that oxidizes on AgO_x (~38%) is approximately equal to the local coverage of oxygen in the initial AgO_x layer ($[O] = 0.38$ to 0.40 ML) for Pd coverages below ~0.7 ML. This correspondence is intriguing since it suggests that the local AgO_x to Pd O-transfer process reaches complete conversion at 300 K; all of the O-atoms in the vicinity of the deposited Pd migrates from the AgO_x phase and oxidizes the Pd. The morphological evolution identified with STM provides further insights for understanding the auto-oxidation of Pd on the AgO_x layer. Specifically, the XPS results suggest that O-transfer may be confined to the buried Pd-AgO_x interface when Pd grows as single-layer domains at $[Pd] < 0.15$ ML. Since nominally 100% of the Pd atoms is in direct contact with the AgO_x phase for single-layer Pd growth, the fraction of Pd

atoms that oxidizes would equal the local O-coverage in the AgO_x layer if only oxygen at the buried Pd- AgO_x interface oxidizes the Pd. STM images support this conclusion since they reveal minimal disruption of the surrounding AgO_x structure after deposition of low Pd coverages (< 0.15 ML) when single-layer growth dominates (e.g., Figure 3a).

Similar considerations suggest that O-atoms from the surrounding AgO_x surface are needed to account for the amount of Pd that oxidizes during bi-layer Pd growth. Again, XPS shows that the fraction of oxidized Pd remains equal to the local oxygen coverage in the AgO_x layer as the Pd coverage increases to at least 0.66 ML. However, STM shows that bi-layer Pd clusters become dominant at Pd coverages above 0.15 ML (e.g., Table 1, Figure 3b), meaning that only about half of the Pd atoms make direct contact with the AgO_x layer. Thus, the oxygen involved in oxidizing the second layer Pd must originate from areas of the AgO_x phase that are not covered by Pd, i.e., located outside of the buried Pd- AgO_x interface. STM images support this interpretation since they provide evidence that the surrounding AgO_x layer undergoes restructuring after the formation of bi-layer clusters at Pd coverages greater than or equal to 0.30 ML (e.g., Figure 3b). Taken together, the STM and XPS results demonstrate that the auto-oxidation of Pd by AgO_x is highly efficient and involves O-transfer to Pd at the buried Pd- AgO_x interface as well as O-migration from uncovered AgO_x regions during bi-layer cluster growth. These oxygen transfer processes may influence the single to bi-layer transition but their exact role is unclear.

Discussion

Our results show that oxygen migrates efficiently from AgO_x to Pd deposits and that strong interactions with the AgO_x layer influence the growth and morphology of deposited Pd clusters.

The higher oxophilicity of Pd over Ag³¹ creates a gradient in the oxygen chemical potential after depositing Pd on the AgO_x film that stimulates the oxygen transfer. The greater stability of PdO_x, and chemisorbed O on Pd, compared with the AgO_x single-layer is also evident from prior O₂ TPD studies, which report that oxygen desorbs from Pd and Pd oxides at temperatures (~650-850 K)^{32, 33} that are significantly higher than that at which the AgO_x single-layer layer decomposes during TPD (~570 K).^{16, 22, 34} The present results demonstrate that the kinetics of AgO_x to Pd O-migration processes are highly facile as the amount of Pd that oxidizes is equal to the local O-coverage in the AgO_x layer, i.e., the amount of AgO_x that could make direct contact with the Pd transfers all of its oxygen to Pd. Our results also provide evidence that the auto-oxidation of Pd occurs at the buried Pd-AgO_x interface and also via oxygen migration from uncovered AgO_x areas to Pd clusters at Pd coverages above ~0.15 ML.

The morphology of the Pd clusters and the Pd growth mechanism demonstrate that Pd achieves strong adhesion on the AgO_x single-layer. The initial formation of well-dispersed, single-layer Pd clusters on top of the AgO_x layer shows that strong interfacial bonding suppresses the formation of large Pd islands, even though such agglomeration would lower the amount of low-coordination Pd atoms located at the edges of the clusters. The Ag_n units also impart their triangular shape and orientation on the initial single-layer Pd clusters, providing further evidence of a strong Pd-AgO_x interaction that may be mediated by the O-atom rows separating the Ag_n units. The transition to bi-layer growth at relatively low Pd coverage suggests a complex interplay between O-transfer to Pd and continued wetting of Pd on the AgO_x layer. Single-layer Pd domains would be expected to continue to develop at high Pd coverage if O-atoms in the AgO_x layer simply strengthened Pd binding to the surface. Instead, our results suggest that the formation of partially-oxidized Pd bi-layer clusters with concomitant reduction of the surrounding AgO_x, becomes favored over single-

layer Pd formation once the density or sizes of single-layer Pd clusters increase sufficiently. Oxygen transfer from AgO_x to Pd likely plays a central role in mediating the transition from single to bi-layer Pd growth. Determining the factors responsible for the single to bi-layer transition will require computational studies to explore the energetics of various Pd- AgO_x structures as well as pathways for their formation.

Summary

We investigated the growth and auto-oxidation of Pd deposited onto single-layer $\text{AgO}_x/\text{Ag}(111)$ using STM and XPS. Palladium forms well-dispersed, single-layer structures up to a Pd coverage of ~ 0.15 ML that adopt the shapes and orientations of triangular Ag_n units in the underlying AgO_x layer. Bi-layer clusters preferentially form upon increasing the Pd coverage to 0.30 ML, and develop into a nearly conformal film as the Pd coverage reaches 1.8 ML. XPS demonstrates that the AgO_x layer efficiently transfers oxygen to the deposited Pd at 300 K. Quantitative analysis of the XPS Pd 3d spectra shows that the fraction of oxidized Pd is equal to the local O-atom coverage in the AgO_x layer for Pd coverages up to at least ~ 0.7 ML. These results demonstrate that the higher oxophilicity of Pd over Ag produces a strong interaction between Pd and the AgO_x layer that influences the morphological evolution and promotes auto-oxidation of the deposited Pd. The ability to generate Pd- AgO_x surfaces with highly dispersed single or bi-layer Pd clusters could provide opportunities for investigating cluster size effects in the chemistry promoted by PdAg bimetallic surfaces. The present results also suggest the possibility that oxygen transfer from Ag to Pd could play a role in mediating chemical reactions of adsorbed molecules on bimetallic PdAg surfaces under oxidizing conditions.

Acknowledgements

The authors thank Abdulrahman Almithn for generating model representations of the AgO_x structures. This work was supported as part of the Integrated Mesoscale Architectures for Sustainable Catalysis, an Energy Frontier Research Center funded by the U.S. Department of Energy, Office of Science, Basic Energy Sciences under Award No. DE-SC0012573.

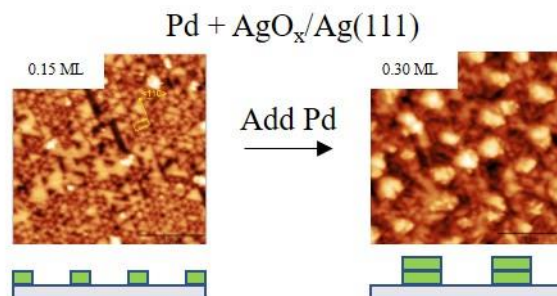
Supporting Information

O₂ TPD and LEED after Ag(111) oxidation with ozone vs. atomic oxygen; LEED from single-layer AgO_x/Ag(111) at 500 K vs. flashing to 520 K; High resolution STM image from 0.04 ML Pd-AgO_x/Ag(111); Analysis of STM images; XPS spectra from Pd-AgO_x/Ag(111) surfaces.

References

1. G. Lapisardi, P. Gelin, A. Kaddouri, E. Garbowski and S. Da Costa, *Top. Catal.*, 2007, 42-43, 461-464.
2. G. Lapisardi, L. Urfels, P. Gelin, M. Primet, A. Kaddouri, E. Garbowski, S. Toppi and E. Tena, *Catal. Today*, 2006, 117, 564-568.
3. J. F. Weaver, *Chem. Rev.*, 2013, 113, 4164-4215.
4. G. S. Jones, M. A. Barteau and J. M. Vohs, *J. Phys. Chem. B*, 1999, 103, 1144-1151.
5. G. S. Jones, M. A. Barteau and J. M. Vohs, *Surf. Sci.*, 1999, 420, 65-80.
6. A. Klust and R. J. Madix, *Surf. Sci.*, 2006, 600, 5025-5040.
7. A. Klust and R. J. Madix, *J. Am. Chem. Soc.*, 2006, 128, 1034-1035.
8. I. E. Wachs and R. J. Madix, *Surf. Sci.*, 1978, 76, 531-558.
9. M. A. van Spronsen, K. Daunmu, C. R. O'Connor, T. Egle, H. Kersell, J. Oliver-Meseguer, M. B. Salmeron, R. J. Madix, P. Sautet and C. M. Friend, *J. Phys. Chem. C*, 2019, 123, 8312-8323.
10. L. E. Walle, H. Gronbeck, V. R. Fernandes, S. Blomberg, M. H. Farstad, K. Schulte, J. Gustafson, J. N. Andersen, E. Lundgren and A. Borg, *Surf. Sci.*, 2012, 606, 1777-1782.
11. F. Zhang, L. Pan, T. Li, J. Diulus, A. Asthagiri and J. F. Weaver, *J. Phys. Chem. C*, 2014, 118, 28647-28661.
12. S. P. Devarajan, J. A. Hinojosa and J. F. Weaver, *Surf. Sci.*, 2008, 602, 3116-3124.
13. C. J. Powell and A. Jablonski, in *National Institute of Standards and Technology*, Gaithersburg, Maryland 20899, 2010.
14. S. Doniach and M. Sunjic, *Journal of Physics Part C Solid State Physics*, 1970, 3, 285-&.

15. D. A. Shirley, *Phys. Rev. B*, 1972, 5, 4709-&.
16. J. Derouin, R. G. Farber, M. E. Turano, E. V. Iski and D. R. Killelea, *ACS Catal*, 2016, 6, 4640-4646.
17. J. Schnadt, J. Knudsen, X. L. Hu, A. Michaelides, R. T. Vang, K. Reuter, Z. S. Li, E. Laegsgaard, M. Scheffler and F. Besenbacher, *Phys. Rev. B*, 2009, 80.
18. J. Schnadt, A. Michaelides, J. Knudsen, R. T. Vang, K. Reuter, E. Laegsgaard, M. Scheffler and F. Besenbacher, *Phys. Rev. Lett.*, 2006, 96.
19. M. Schmid, A. Reicho, A. Stierle, I. Costina, J. Klikovits, P. Kostelnik, O. Dubay, G. Kresse, J. Gustafson, E. Lundgren, J. N. Andersen, H. Dosch and P. Varga, *Phys. Rev. Lett.*, 2006, 96.
20. N. M. Martin, S. Klacar, H. Gronbeck, J. Knudsen, J. Schnadt, S. Blomberg, J. Gustafson and E. Lundgren, *J. Phys. Chem. C*, 2014, 118, 15324-15331.
21. J. Knudsen, N. M. Martin, E. Granas, S. Blomberg, J. Gustafson, J. N. Andersen, E. Lundgren, S. Klacar, A. Hellman and H. Gronbeck, *Phys. Rev. B*, 2011, 84.
22. J. Derouin, R. G. Farber, S. L. Heslop and D. R. Killelea, *Surf. Sci.*, 2015, 641, L1-L4.
23. L. A. Mancera, R. J. Behm and A. Gross, *Phys. Chem. Chem. Phys.*, 2013, 15, 1497-1508.
24. A. K. Engstfeld, H. E. Hoster and R. J. Behm, *Phys. Chem. Chem. Phys.*, 2012, 14, 10754-10761.
25. Y. S. Ma, T. Diemant, J. Bansmann and R. J. Behm, *Phys. Chem. Chem. Phys.*, 2011, 13, 10741-10754.
26. Y. Ma, J. Bansmann, T. Diemant and R. J. Behm, *Surf. Sci.*, 2009, 603, 1046-1054.
27. G. Ketteler, D. F. Ogletree, H. Bluhm, H. J. Liu, E. L. D. Hebenstreit and M. Salmeron, *J. Am. Chem. Soc.*, 2005, 127, 18269-18273.
28. J. F. Weaver and G. B. Hoflund, *Chem. Mater.*, 1994, 6, 1693-1699.
29. J. F. Weaver and G. B. Hoflund, *J. Phys. Chem.*, 1994, 98, 8519-8524.
30. P. Pervan and M. Milun, *Surf. Sci.*, 1992, 264, 135-146.
31. G. V. Samsonov, *The Oxide Handbook*, Plenum Press, London, 1973.
32. H. H. Kan, R. B. Shumbera and J. F. Weaver, *Surf. Sci.*, 2008, 602, 1337-1346.
33. H. H. Kan and J. F. Weaver, *Surf. Sci.*, 2009, 603, 2671-2682.
34. C. T. Campbell, *Surf. Sci.*, 1985, 157, 43-60.



Pd is auto-oxidized during deposition onto AgO_x and undergoes a transition from single to bi-layer growth at low Pd coverage.